Original Article
ISSN (Online): 2456-8651

International Journal of Engineering Science Technologies
September-October 2024 8(5), 1–19

COMPARATIVE STUDY USING CFD OF COUNTER-CURRENT AND CO- CURRENT HYDROTREATING REACTORS USING JATROPHA CURCAS L VEGETABLE OIL

Pablo Vizguerra Morales [1], Fabian S. Mederos Nieto [1]

[1] Centro Mexicano para la Producción más Limpia (CMPL), Instituto Politécnico Nacional Ciudad de México, México

Received 15 August 2024
Accepted 17 September 2024
Published 15 October 2024

Corresponding Author

Pablo Vizguerra Morales,
p.vizguerramorales@ugto.mx

DOI 10.29121/IJOEST.v8.i5.2024.635

Funding: This research received no specific grant from any funding agency in the public, commercial, or not-for-profit sectors.

ABSTRACT

In this work, mathematical modeling and CFD simulation of two countercurrent and cocurrent hydrotreatment reactors were carried out, validating the results with a drained bed reactor (TBR), a commercial CoMo/γ-Al2O3 catalyst was used, the material the raw material was Jatropha Curcas L vegetable oil. The operating conditions were temperature 380 ° C, pressure 8 MPag. The kinetic model that was used considered 13 reactions that involve processes of decarboxylation, decarbonization, hydrodeoxygenation and hydrocracking reactions for triolein and tristearin triglycerides. The CFD simulation was carried out in Fluent 18.2 in a transient state and in 3D, considering the standard κ - ε turbulence models, Eulerian multiphase model and porous medium model, it was shown that the countercurrent reactor has less pressure drop than the countercurrent, the conversion the countercurrent reactor has a greater conversion of reactants of 99%, the generation of products from the countercurrent reactor has higher concentrations than the cocurrent reactor, this is because it has more contact areas between phases in the reactor.

Keywords: Countercurrent Reactor, Cocurrent Reactor, CFD, Biofuels

1. INTRODUCTION

In recent years, energy demand has been increasing worldwide, especially in Mexico, in the coming years, after 2030, is expected to increase due to population growth and the development of society. One of the main sources of energy generation to satisfy current needs are fossil fuels, which cause the emission of CO2, SO2 and other polluting gases, which lead to environmental problems such as; climate change and global warming that seriously affects us with droughts and intense heat throughout the country. A & M (2007)Therefore, it is important to

counteract the environmental impact and generate alternative fuel sources to satisfy this demand.

It is very important to use renewable energies such as wind, solar and biofuels since it is an alternative source of energy due to its sustainability and low emissions of CO2, CO, SO2 and particulate matter. These biofuels result mainly from biomass raw materials, such as non- edible vegetable oils, sunflower oil and palm oil, etc. The advantages of biomass are that they are free of sulfur, nitrogen and ash; Thus, its emissions are also free of SOx, NOx and CO2.Anand & Sinha (2012).

Biofuels are presented as an option for the sustainable development of the country through a new option for the energy matrix, as well as an instrument for moderating climate change and global warming.

Biofuels are classified as advanced renewable biofuels, this classification depends mainly on the type of raw material, conversion technology, product formed and carbon source Gallakota (2015). Bioethanol and biodiesel are first generation biofuels derived from biomass, while second generation biofuels are derived from lignocellulosic biomass. The main obstacle is the degradation of biomass. F. H. Mahfud. (2007)

The bio-oil obtained from the pyrolysis of lignocellulosic biomass is unstable and has a high water content, low pH, high viscosity, low heating value, and is highly corrosive. The bio-oil produced has 300 different organic compounds, mostly consisting of (20-30% by weight) water, (15-30% by weight) lignin fragments, (10-20% by weight) aldehydes, (10-15% by weight) carboxylic acids, (5-10% by weight) carbohydrates, (2-5% by weight) phenols, (1- 4% by weight) furfurals, (2-5% by weight) alcohols and ketones (1-5% by weight), Oasmaa (2002).

The deterioration of biomass oil properties due to pyrolysis, an improvement and optimization process is required. Currently, there are several techniques available to transform bio-oils into fuels, these are catalytic hydrodeoxygenation Furimsky (2002), zeolite upgrading Adjaye (1995), catalytic cracking Hew (2010), supercritical technology Tang (2009) and emulsification Bridgwater (2002). The first review on the compliance of the bio-oil improvement process through HDO was explained by Furimsky, he worked with a tubular reactor in cocurrent mode and determined the rate constants, problems associated with the presence of oxygen and the growing concern about the improvement of fuels derived from coal and biomass Furimsky (1983).

This led to a paradigm shift in research towards techniques related to the improvement of bio-oils. Oyama reported that the HDO process is similar to hydrodenitrogenation (HDN) but 10 times more efficient than the later technique on vanadium nitride catalysts, Oyama (1996). Maggi and Delmon published a review on aspects related to the catalytic chemistry, kinetics and reaction mechanisms of HDO using oxygenated compounds, Maggy (1997), It was used a fixed bed tubular reactor with continuous flow, Senol (2007).

In other study carried out semi-batch HDO experiments using acetic acid and furfural to represent pyrolysis products of hemicellulose and cellulose, respectively, in the absence of catalyst, reporting the formation of a solid furfural polymeric material at 250 °C, Elliott (2009), Using Ru/C as the catalyst and acetic acid as the feed, they observed negligible conversions at low temperatures (< 200 °C) and strong gas production at high temperatures (> 250 °C), their approach resulting in a reduction in oxygen content. from 41.3% by weight to 20-27.0%.

Another study developed a mathematical model for a new industrial-scale three-phase catalytic radial flow reactor (RFR), which was developed using a two-

dimensional mixing cellular network (MCN) model. RFR is used for gas phase reactions in the petroleum refining

industry. This work analyzes the capabilities of three-phase RFR for diesel hydrodesulfurization, Yadav (2022). The reactions considered for the development of the diesel hydrodesulfurization model are hydrodesulfurization, hydrodearomatization and olefin saturation. Apart from the well-known advantage of RFR such as pressure drop, other benefits such as better product quality, reduced H2S inhibition, no need for quenching.

Jinjin Liu work on the liquid phase maldistribution factor in a trickling bed reactor and the results are compared with measurement data by using electrical resistance tomography, Liu (2020). The simulation results agree with the experimental results to a certain extent. Another study used four-element computational fluid dynamics (CFD) a model was proposed for the investigation of vacuum gas oil with hydrocracking in a trickle bed reactor, Faraji (2020). The experiment was at 360–390 °C and 146 bar in the reactor at three different flow rates. J. & Farchad (2009).

Another work was in steady-state operation mode of the countercurrent reactor of a heterogeneous liquid-liquid system, Andrianova (2014), a two-temperature model of the countercurrent plug flow reactor is developed for two liquids that chemically interact l, the dispersion medium (continuous) and the dispersed phase. It is shown that the degree of localization is greater the greater the reaction speed.

Alex A.J. Breije work on preventing drip bed flooding in a counterflow reactor using additional void space. The influence of additional void space (AVS) configuration on the flooding point and gas-liquid mass transfer coefficient (kLa) of structured packings have been investigated in a countercurrent trickling bed reactor, Breije (2018).

Another study focused on the mathematical modeling of a hydrocracking reactor for the conversion of triglycerides into biofuel. In the study, a 2D, non-isothermal and heterogeneous model of a triglyceride hydrocracking reactor is investigated, the energy conservation equations and mass were solved simultaneously using appropriate numerical techniques whose reliability was evaluated by comparing the results with experimental data. Calculations indicated that at a feed temperature of 380 °C, a liquid hourly space velocity of 8 h−1, and a hydrogen: feed ratio of 1500:1, the total triglyceride conversion was 82.54% for the four classes. main hydrocarbons (light, medium, heavy and oligomerized), Forghani (2014). Edward Furimsky. (1983)

Another work was the CFD simulation of porosity and particle diameter Influencing the wall to heat transfer bed in drip bed reactors, Heidari (2019). In this study, the hydrodynamics and thermal behavior of trickle-bed reactors were simulated using computational fluid dynamics (CFD) technique.

Paweł work on an interfacial heat transfer in a countercurrent gas-liquid flow in a trickle bed reactor, the lack of correlations describing the interfacial gas-liquid heat transfer coefficient creates problems when developing numerical models of non-current flows. isothermal in porous media, Niegodajew (2017). Therefore, the experimental investigation was carried out with the use of a 0.1 m inner diameter column, equipped with 6 mm glass Raschig rings. Media loadings ranged from 0.0177 to 0.1415 m3 (m2 s) -1 and 0.0007–0.0053 m3 (m2 s) -1

for the gas and liquid phases, respectively. The results of the experiment were used to develop a new correlation that described the interphase heat transfer in the packed bed expressed by the Nusselt number.

Another work focused on the simulation and optimization of a hydrotreating reactor using a new adaptive hybrid algorithm based on the neuro-fuzzy inference imperialist competition system (ICA-ANFIS), in the optimal result, sulfur removal increased by a 33% compared to baseline, Eshghanmalek (2022).

Silva work on the use of CFD to investigate the hydrotreatment of diesel hydrodesulfurization (HDS) and Hydrodesaromatization (HDA) in a laboratory-scale trickling bed reactor (TBR). To investigate these reactions, the 3D model was developed using a multi-phase Eulerian approach, a phase interaction model, a porosity distribution model for trilobe particles, mass transfer model and chemical reactions, Silva (2017). Another study involved the modeling and simulation of maldistribution flow in randomly packed columns with gas-liquid countercurrent flow. The simulation results agree well with the experimental results obtained in our laboratory for both water/air and isopar/air systems, Sun (2000).

Uribe worked on the CFD analysis of the textural characteristics of the bed in TBR behavior: Kinetics, scaling, multiscale analysis and wall effects, Uribe (2019). The CFD results were validated against experimental pressure drop data as well as theoretical HDS and HDN conversion data. Muharam worked on modeling a hydrotreating reactor to produce renewable diesel from non-edible vegetable oils using CFD, Muharam (2017). Another study by Muharam was on predicting the effects of inlet velocity and reactor length on the performance of a trickle bed reactor for the production of renewable diesel.

Another study was to describe a model to predict the behavior of trickling bed reactors used for catalytic hydrotreatment of petroleum fractions with countercurrent and cocurrent modes of operation. Superior performance was found in a countercurrent mode of operation over the cocurrent mode. It was recognized that the countercurrent mode may have great potential to be used for deep hydrodesulfurization of petroleum fractions since it minimizes the inhibitory effect of some products (e.g., H2S) in the reactor zones where these species tend to concentrate in the concurrent mode, Muharam & Yuswan (2019)

1.1. THEREFORE, THIS WORK HAS THE OBJECTIVE:

Find the mathematical model of hydrodynamics and mass transport in countercurrent and cocurrent hydrotreating reactors using Fluent and will be validated with experimental data from the TBR reactor and analyze which of the reactors is best for us in terms of operation and conversion of products for its industrial scale.

1.2. PROBLEM STATEMENT

The reactors that were simulated is a microscale was two countercurrent and cocurrent hydrotreatment reactors with a diameter of 1.3 cm and a height of 30 cm. It was simulated in Fluent 18.2 and is shown in Figure 2 The operating conditions that were considered for the simulation were temperature 380 °C, pressure 8 MPag, LHSV 8.0 h−1.

The results were validated with the experimental results with a The dynamic drained bed reactor (TBR) for the hydrotreatment process, which was used experimentally with a commercial CoMo/γ-Al2O3 catalyst, Jatropha Curcas L

vegetable oil was used as raw material, is shown in Figure 1, Mederos Nieto et al. (2020)

Figure 1

Figure 1 Experimental HDO Reactor

The dimensions and operating conditions of the TBR reactor are shown in Table 1 and the conditions to be simulated in countercurrent and cocurrent modes are also shown.

Table 1

Table 1 Reactor Conditions and Operation

Reactor	
Scale	Micro
Mode to Simulate	Countercurrent and cocurrent Isothermal
Type	
Operation variables	
Pressure (bar)	8
Temperature (°C)	320- 380
H2/ Oil volume ratio (NL/L)	1000-1500
Gas Phase	
Mass flow (Kg/s)	4.8 x10 -6
Composition (%mol)	100
Liquid phase	
Mass flow (Kg/s)	1.1 x10 -6
Composition (% mol)	10
Solid phase	
Particle shape	trilobular
Catalyst mass (g)	2
Catalyst volume (cm3)	2.4
Inert volume (cm3)	2.4
Bed volume (cm3)	3.7165

Bed length (cm)	2.8
Equivalent particle diameter (cm)	0.052
Reactor dimensions	
Diameter (cm)	1.3
Total length (cm)	30

2. GOVERNMENT EQUATION

The following equations are those involved in solving the problem posed by the physical phenomenon to be modeled: Reynolds average Navier-Stokes (RANS) equation, turbulence model standard $(k-\varepsilon)$, equations of state and coupled methods; FLUENT uses the finite

volume method as a numerical method to solve the governing equations and those mentioned above, Ansys (2018).

The partial differential equations that describe the phenomenon of mass transport are the following:

The conservation of mass or continuity equation.

$$\frac{\partial \rho}{\partial t} + (\nabla . \rho v) = S_m \tag{1}$$

The above equation is the general form of the mass conservation equation and is valid for incompressible as well as compressible flows. The term $(\nabla . \rho v)$ is called divergence of ρv This is the matter flux density vector and represents the rate at which the matter flux density decreases per unit volume. The term source Sm is the mass added to the continuous phase from the dispersion of a second phase (e.g., due to vaporization of liquid particles).

The conservation of momentum in an inertial (non-accelerated) reference frame is described by the equation.

$$\frac{\partial}{\partial t}(\rho v) = -\nabla \cdot (\rho v v) - \nabla p - \nabla \cdot \tau + \rho g + F \tag{2}$$

where p is the static pressure, $\bar{\bar{\tau}}$ is the stress tensor, $\rho g^{\rightarrow}$ is the gravitational force and $F^{\rightarrow}$ is the external force. The stress tensor is given by:

$$\tau = \mu \left[\left(\nabla \vec{v} + \nabla \vec{v}^{T} \right) - \frac{2}{3} \nabla . \vec{v} I \right] \tag{3}$$

Where μ is the molecular viscosity, I is the unit tensor and the second term on the right side is the effect of volume expansion. Standard turbulence model $(k-\varepsilon)$

$$\frac{\partial}{\partial t}(\rho k)+\frac{\partial}{\partial x_i}(\rho k u_i)=\frac{\partial}{\partial x_j}\left(\left(\mu+\frac{\mu_t}{\sigma_k}\right)\frac{\partial k}{\partial x_j}\right)+G_k+G_b-\rho\varepsilon-Y_M \quad (4)$$

$$\frac{\partial}{\partial t}(\rho \varepsilon)+\frac{\partial}{\partial x_i}(\rho \varepsilon u_i)=\frac{\partial}{\partial x_j}\left(\left(\mu+\frac{\mu_t}{\sigma_\varepsilon}\right)\frac{\partial \varepsilon}{\partial x_j}\right)+C_{1\varepsilon}\frac{\varepsilon}{k}(G_k+C_{3\varepsilon}G_b)-C_{2\varepsilon}\rho\frac{\varepsilon^2}{k} \quad (5)$$

$$\mu_t=\rho C_\mu\frac{k^2}{\varepsilon} \quad (6)$$

The above equations are considered in cartesian coordinates, C1, C2, C3, σk, y σε are closure coefficients for the standard turbulence model (κ - ε) equations 5 and 6. The values of these coefficients are:1.44, 1.92, 0.09, 1.0 y 1.3, respectively.

The energy conservation equation is given by the following expression:

$$\frac{\partial}{\partial t}(\rho E)=-\nabla\cdot\left(\vec{v}(\rho E)\right)-(\nabla\cdot q)+\rho(v.g)-(\nabla\cdot pv)-(\nabla\cdot[\tau.v])+S_h \quad (7)$$

Porous media models for single-phase and multiphase flows use a pore surface velocity formula as the default option. ANSYS Fluent calculates surface phase or mixing rates based on volumetric flow rate in a porous region. The pore surface velocity formulation generally provides good representations of the pressure loss through a porous region. In the Eulerian model, a series of n heat and momentum continuity equations are solved for each phase, coupling the phases through pressure and exchange coefficients between phases. The way this coupling is handled depends on the type of phases involved; for granular flows the properties are obtained from the application to kinetic theory.

The countercurrent and cocurrent reactors that were simulated in CFD are shown in Figure

2. To analyze the operation of both reactors, the CFD tool can be used to predict and analyze the operation and behavior of these reactors, to find the best option for the reactor. HDT process and scale to an industrial level.

Figure 2

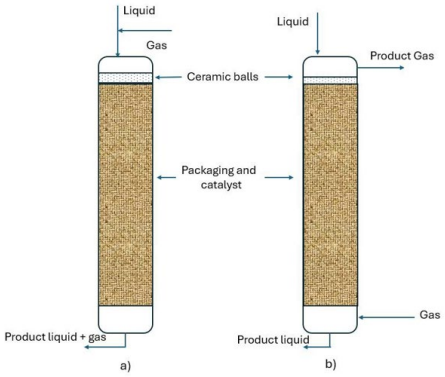

Figure 2 Schematic Diagrams of Fixed Bed Catalytic Reactors: A) Cocurrent Reactor And B) Countercurrent Reactor

3. KINETIC MODEL

The proposed mathematical model considers the hydrotreatment of Jatropha Curcas L. vegetable oil, whose experimental data have been reported in the literature. The raw material contains more than 95% triglycerides, the rest corresponds to small amounts of monoglycerides, diglycerides and free fatty acids. For this study we took the hydrotreatment of 2 main triglycerides which are; triolein and tristearin, taking into account their decarboxylation, decarbonylation and hydrodeoxygenation reactions.

The global direct kinetics of HDC and oligomerization of Jatropha oil, where the components produced within the HDC reaction were classified into 5 groups: reactive (TG), light, LP (nC5– C8), medium, MP (nC9- C14), heavy, HP (nC15-C18) and oligomerized, OP (> nC18), are shown in the kinetic model (Fig.3), Anand and Sinha (2012).

Figure 3

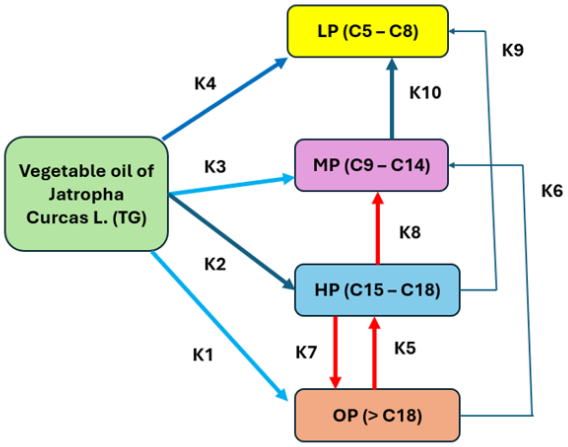

Figure 3 Kinetic Model for the Hydroconversion of Triglycerides

Table 2shows the temperature-dependent kinetic parameters for each reaction determined with the Arrhenius equation, that is, its activation energy and its pre-exponential factor.

Table 2

Table 2 Arrhenius kinetic parameters of the HDT of Jatropha vegetable oil

Reaction j	Aoj(h-1)	EAj (Kj/mol)	R2
Tg - Ol (1)	9.8723×10^{9}	128.4918	0.636
Tg - Hv (2)	157.5599	12.7951	0.992
Tg - Md (3)	1.1004×10^{21}	277.9029	0.987
Tg - Lh (4)	3.4066×10^{9}	127.7768	0.983
Ol - Hv (5)	127.1923	20.7014	0.781
Ol - Md (6)	-	-	-
Hv - Ol (7)	6.1409×10^{12}	173.1821	0.975
Hv - Md (8)	1.3894×10^{19}	260.85	0.953
Hv - Lh (9)	0.0424	2.1775	0.952
Md - Lh (10)	0.2817	6.5759	0.954

4. MATERIALS AND METHODS

The study of hydrodynamics and mass transfer was carried out with CFD tools in Fluent 18.2, which will give us contours and profiles of pressure, temperature and products obtained for the countercurrent and cocurrent reactor. A computer with 12 GB RAM and an Intel 7.0 processor was used. The essential steps to carry out a study of this type were to obtain an appropriate mesh for both reactors, propose models and the solver to represent our process and the analysis of results.

4.1. CFD SIMULATION

4.1.1. PREPROCESSING

The meshing of the countercurrent and cocurrent reactor was performed in the ANSYS ICEM software and the boundary conditions were also introduced to the mesh.

1) The mesh for the countercurrent reactor was made with structured meshing, that is, with hexahedral cells with a size of 52003 cells, and for the cocurrent reactor, it was also meshed with hexahedral cells with a size of 52005 cells, shown in Figure 4

Figure 4

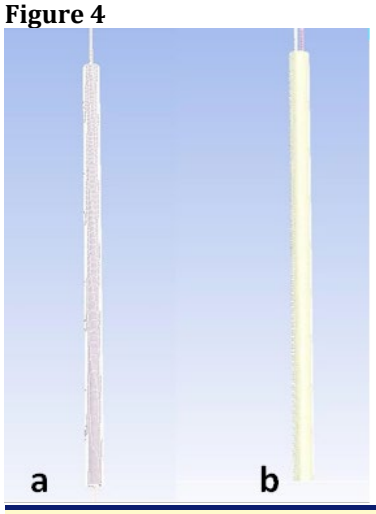

Figure 4 A) Mesh Generated for the Countercurrent Reactor And B) Mesh Generated for the Cocurrent Reactor

Las condiciones de frontera se muestran en la Figura 5 para el reactor a contracorriente y cocurrente.

4.2. PROCESSING

2) The simulation in Fluent 18.2 was carried out in 3 dimensions, in steady and transient states, using the viscous model of estándar k □ □ , the Eulerian multiphase model, for the gas, liquid and solid phases and the Porous Medium model.
3) The boundary conditions used in Fluent are shown in Table 3, for both countercurrent and cocurrent reactors.
4) The convergence criteria were 0.001 for all equations, for 3600 seconds of simulation.

Figure 5

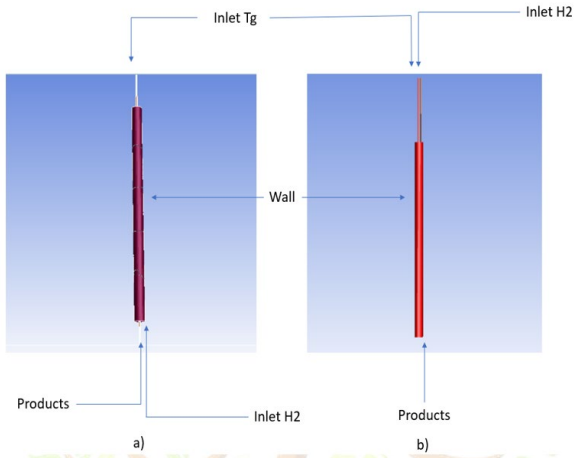

Figure 5 The Boundary Conditions for Both Reactors; A) Countercurrent and B) Cocurrent

Table 3

Table 3 Boundary Conditions for CFD Simulation

Zones	Boundary condition	Values	Pressure (Pa)	Temperature(°K)	Species (mole fraction)
Oil inlet (TG)	Mass flow (kg/s)	4.80E-06	100	330	0.0006
H2 inlet	Mass flow (kg/s)	1.10E-06	200	325	1
Gas product outlet	outlet pressure (Pa)	0	0	750	-
Liquid products output	outlet pressure (Pa)	0	0	750	-
Wall	Wall	Stationary	0	800	-

4.3. POST PROCESSING

5) The temperature and pressure profiles and contours of both reactors will be obtained, as well as the speed profiles within them, the profiles of the

reactants and products will be obtained, as well as the triglyceride conversion profiles, the mathematical model will be validated in Fluent with experimental data carried out in operating reactor.

5. RESULTS AND DISCUSSIONS

The simulation and conversion analysis of the reaction was carried out in the countercurrent and cocurrent reactor using Jatropha oil and hydrogen as raw materials.

Figure 6 shows the pressure contour in the countercurrent reactors a) and cocurrent b) with a simulation of 3600 seconds. For the countercurrent reactor there is a total pressure of 2.68 x 105 Pa and it drops to 2.6 x 104 Pa and for The cocurrent reactor has a total pressure of 2.07 x105 Pa, and it drops to 1.98 x105 Pa, which indicates that in the cocurrent reactor there is more pressure drop, because there is more contact between phases in the countercurrent reactor and why there is more loss of speed in the pores of the reactor.

Figure 6

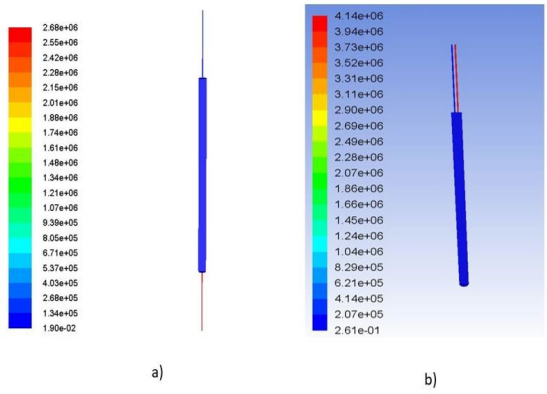

Figure 6 Total Pressure Contour for A) Countercurrent Reactor and B) Cocurrent Reactor

Figure 7 shows the speed magnitude contour in the countercurrent reactors a) and cocurrent b), with a simulation of 3600 seconds, for the countercurrent reactor it has a speed magnitude of 1.25 x10-2 m/s, and for The cocurrent reactor has a speed magnitude of 1.45 x10-2 m/s, which indicates that the countercurrent reactor has a lower speed than the cocurrent reactor, that is, slower and causes a lot of contact between phases. Figure 8 shows the total temperature contour in the countercurrent reactors a) and cocurrent b) with a simulation of 3600 seconds, in the countercurrent reactor there is a total temperature of 775

°K, and for the cocurrent reactor it is observed a total temperature of 794 °K, which indicates that the cocurrent reactor has a higher total temperature than the countercurrent reactor, although the difference is only small and tends to raise the temperature in the cocurrent reactor more.

Figure 9 shows the CO2 contour in the countercurrent a) and cocurrent reactors b), with a simulation of 3600 seconds, the countercurrent reactor has a CO2 mass fraction of 1.21 x 10- 2 and is very low in The entire reactor is only concentrated more at the outlet of the reactor roof and for the cocurrent reactor a mass fraction of 2.89 x 10-3 is observed and is distributed throughout the reactor, which indicates that in the countercurrent reactor it has greater CO2 concentration than the cocurrent reactor.

Figure 7

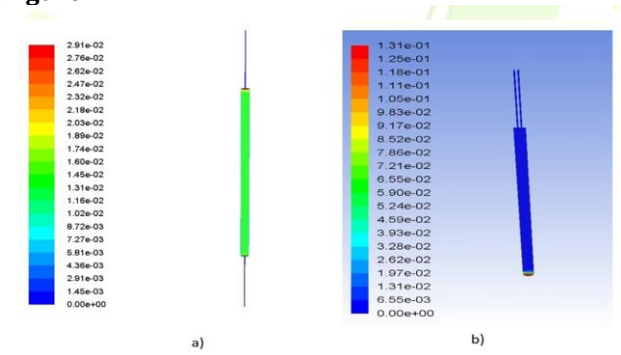

Figure 7 Velocity Magnitude Contour For A) Countercurrent Reactor And B) Cocurrent Reactor

Figure 8

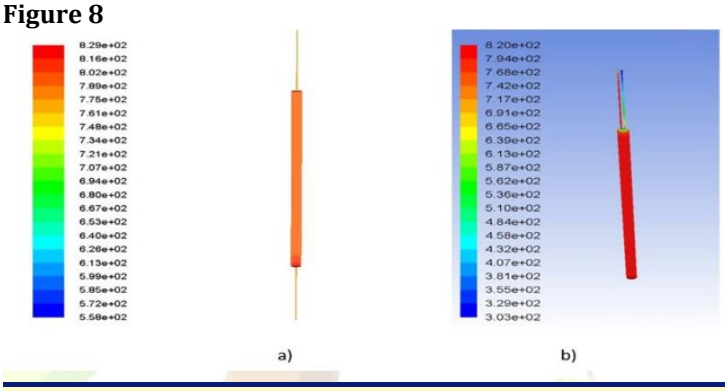

Figure 8 Total Temperature Contour For A) Countercurrent Reactor and B) Cocurrent Reactor

Figure 9

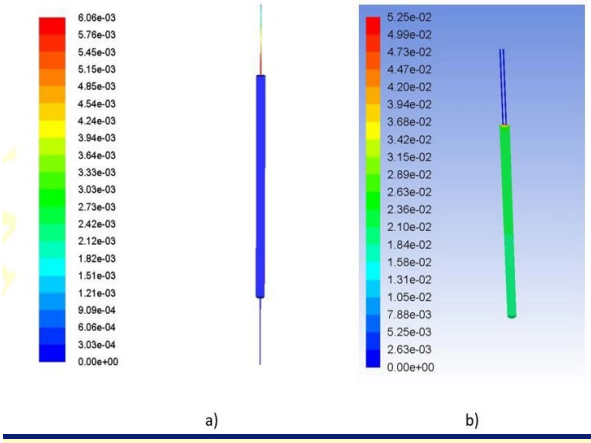

Figure 9 CO2 Mass Fraction Contour For A) Countercurrent Reactor and B) Cocurrent Reactor

Figure 10shows the C3H8 contour (light) in the countercurrent reactors a) and cocurrent b) with a simulation of 3600 seconds. The countercurrent reactor has a mass fraction of C3H8 of 1.15 x 10-1 and remains constant. throughout the entire reactor and for the cocurrent reactor a mass fraction of 1.41 x 10-2 is observed in the lower part and in the central part it has a value of 1.82 x 10-2 and in the upper part with a value of 2.42 x 10-2 which is the maximum value.

Figure 11shows the C4H10 contour in the countercurrent a) and cocurrent reactors b) with a simulation of 3600 seconds. The countercurrent reactor has a mass fraction of C4H10 of 1.36 x 10-1 and remains constant throughout. of the entire reactor and for the cocurrent reactor, a mass fraction of 4.88 x 10-3 is observed in the lower part and in the central part it has a value of 2.68 x 10-3 and in the upper part with a value of 4.88 x 10-4 that is the minimum value, it is concluded that there is more generation of C4H10 because there is more contact of the reactants in the countercurrent reactor.

Figure 12 shows the C9H20 contour in the countercurrent reactors a) and cocurrent b) with a simulation of 3600 seconds. The countercurrent reactor has a mass fraction of C9H20 of 3.62 x 10 -1 and remains constant throughout. of the entire reactor and for the cocurrent reactor a mass fraction of 6.20 x 10-3 is observed in the lower part, in the central part it has a value of 8.86 x 10-3 and in the upper part with a value of 1.68 x 10-2.

Figure 13 shows the C17H36 contour in the countercurrent reactors a) and cocurrent b) with a simulation of 3600 seconds, the countercurrent reactor has a mass fraction of C17H36 of 9.64x 10-2 and remains constant throughout the reactor and for the cocurrent reactor a mass fraction of 1.21x 10-2 is observed and in the central part it has a value of 2.02 x 10-2, in the upper part with a value of 2.22 x 10-2 which is the maximum value.

Figure 10

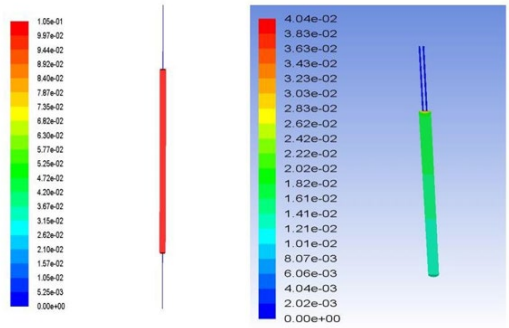

Figure 10 Mass Fraction Contour of C3H8 A) Countercurrent Reactor and B) Cocurrent Reactor

Figure 11

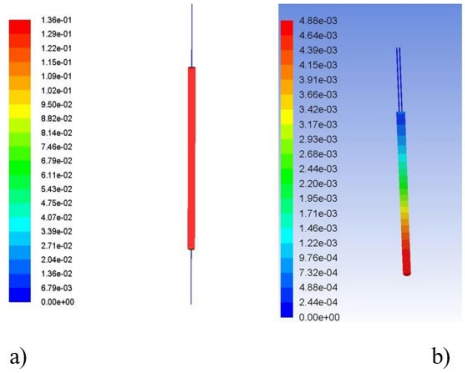

Figure 11 Mass Fraction Contour of C4H10 A) Countercurrent Reactor and B) Cocurrent Reactor

Figure 12

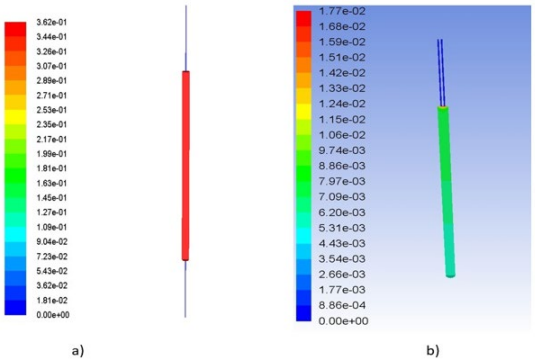

Figure 12 Mass Fraction Contour of C9H20 A) A) Countercurrent Reactor and B) Cocurrent Reactor

Figure 14shows the Ol contour in the countercurrent reactors a) and cocurrent b) with a simulation of 3600 seconds, the countercurrent reactor has a mass fraction of C18H38 of 3.37 x 10-2 and remains constant throughout the reactor and for the cocurrent reactor a mass fraction of 1.48x 10-3 is observed in the lower part, which is the maximum value, and in the central part it has a value of 7.38 x 10- 4, 2.21 x 10-4at the top.

Figure 13

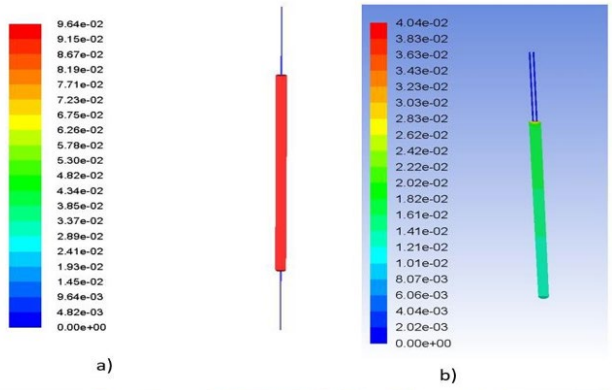

Figure 13 Mass Fraction Contour of C17H36 A A) Countercurrent Reactor and B) Cocurrent Reactor

Figure 14

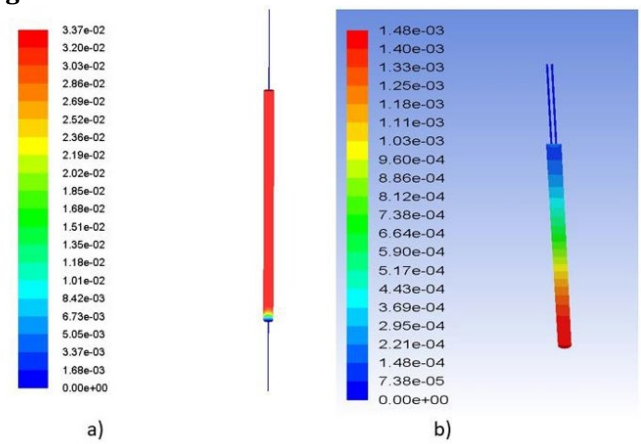

Figure 14 Mass Fraction Contour of Ol A) Countercurrent Reactor and B) Cocurrent Reactor

In this work a comparison is made of the simulation results of both reactors and experimental data from Mederos' work. The comparison of the velocity magnitude profiles in the countercurrent and cocurrent reactors is shown in Figure 15 It is observed that the velocity in the countercurrent reactor ranges from 0.015 to 0.014 m/s and in the cocurrent reactor there is a higher velocity. 0.12 and decreases to 0.003 m/s. The comparison of the total temperature profiles in the countercurrent and cocurrent reactors is shown in Figure 16, it shows that in the cocurrent reactor there is a temperature at the entrance of 795 K and at the exit of 800 K, in the countercurrent reactor at the output has a temperature of 800 K in the 3600 seconds of simulation.

Figure 15

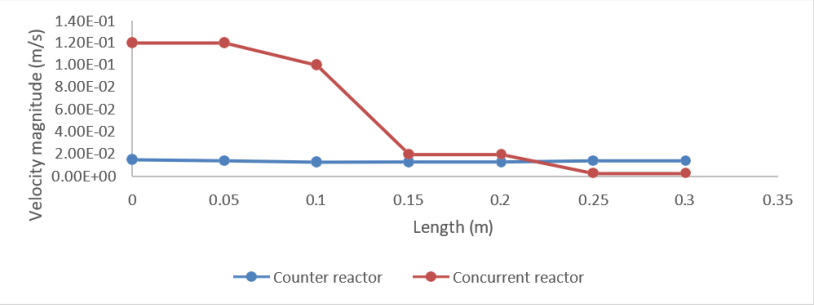

Figure 15 Velocity Magnitude Profiles in Countercurrent and Cocurrent Reactors

Figure 16

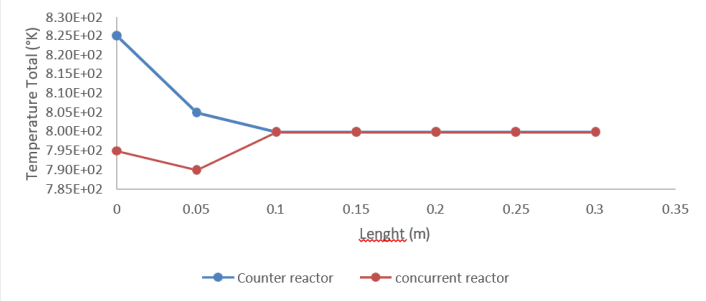

Figure 16 Total Temperature Profiles in Countercurrent and Cocurrent Reactors

Figure 17 shows the retention time that was calculated to be 168.96 seconds for the liquid temperature, and in the simulation, it is observed that it is 200 seconds, because it is where the temperature of the process begins to rise, which shows us that the Simulation adequately represents our process.

The concentrations of light, medium, heavy and oligomerized for the countercurrent reactor are shown in Figure 18 and for the cocurrent reactor are shown in Figure 19 In the countercurrent reactor there are more medium products with an average concentration of 0.525 kmol /m3 of light ones a concentration of 0.107, of heavy ones of 0.0982 and oligomerized of 0.0325. In the cocurrent reactor there are more light products with an average concentration of 0.0227 kmol/m3, medium products with a concentration of 0.00682, heavy products with an average concentration of 0.00419 and oligomerized products with a concentration of 0.0008.

Figure 17

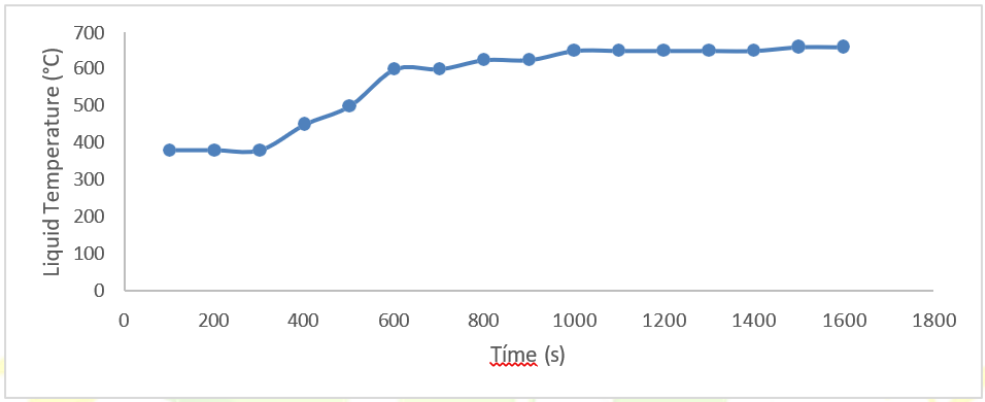

Figure 17 Temperature Profile in Liquid Phase Against Simulation Time at the Bottom of the Countercurrent Micro Reactor

Figure 18

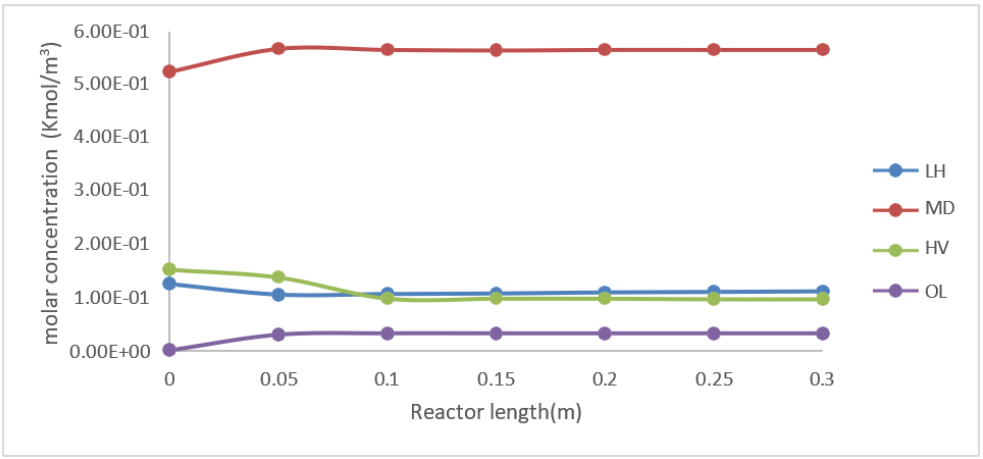

Figure 18 Product Concentration Profile in Countercurrent Reactor

Figure 19

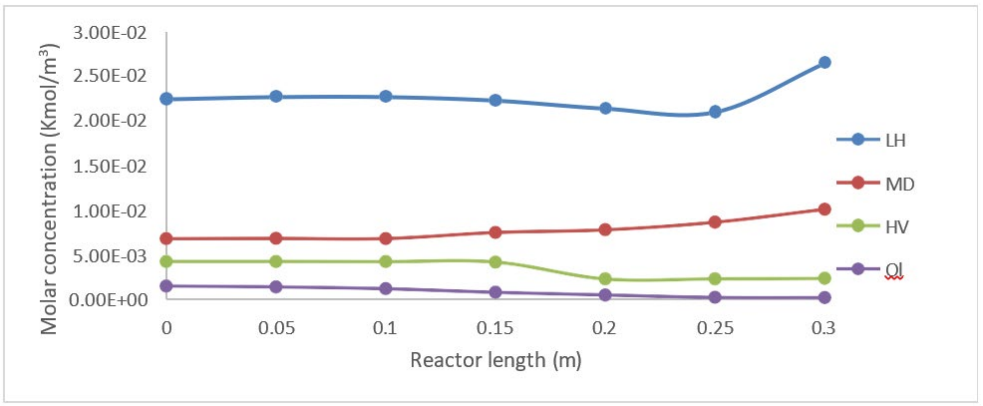

Figure 19 Product Concentration Profile in Cocurrent Reactor

6. CONCLUSIONS AND RECOMMENDATIONS

It is concluded that the mathematical modeling and CFD simulation of the hydrotreatment reactors in countercurrent and cocurrent mode at a microscale level were carried out, these results were validated against the experimental data of the reactor that is in the research center, which is a reactor of drained bed (TBR) having logical and approximate results to the experimental ones.

The process that was simulated in CFD is the hydrotreatment for vegetable oil of Jatropha Curcas L., it was successfully simulated in CFD with the Fluent version 18.2 software. The simulation conditions in Fluent that were considered were; temperature 320–380 °C, pressure 8 MPa, a commercial CoMo/γ-Al2O3 catalyst was used. A reaction mechanism of 13 reactions was considered, only triglycerides were taken into account; triolein and tristearin to produce renewable fuels, the reactions involve decarboxylation, decarbonization, hydrodeoxygenation processes and hydrocracking reactions of triglycerides.

The CFD simulation was carried out in a transient state and in 3 dimensions, considering the standard k-ϵ turbulence model, the Eulerian multiphase model for 3 phases and the porous medium model, obtaining somewhat different results between the countercurrent and cocurrent reactors, in cocurrent there is more depression drop, and greater velocity magnitude than in the countercurrent reactor, in the total temperature both reach a maximum temperature of 800° K. Regarding the operation, it is observed that there is more pressure drop in the countercurrent reactor than in the cocurrent reactor and the total temperature rises a little more in the countercurrent reactor, which is why it is easier to operate the reactor in cocurrent mode.

Taking into account the conversion of products, in the countercurrent reactor more light, medium, heavy and oligomerized products were obtained than in the reactor in cocurrent mode, because in the countercurrent reactor there is more contact between the phases and there is more reaction between the reagents that in the cocurrent reactor, the simulation was carried out for 3600 seconds and a good approximation was observed with the experimental results.

When analyzing which of the reactors is best for us in terms of operation and conversion of products, it is concluded that there is less pressure drop in the cocurrent reactor but there is less conversion of triglycerides and generation of products, on the other hand in the reactor In countercurrent there is more pressure drop and more heating, but there is more conversion of triglycerides and generation of products, which is why the countercurrent reactor is better for us due to its higher conversion of triglycerides. These reactor operating conditions can be brought to an industrial level.

CONFLICT OF INTERESTS

None.

ACKNOWLEDGMENTS

Acknowledge to Dr. Fabian Salvador Mederos Nieto for his support in this work, as well as to the research project SIP - IPN- 20231028.

REFERENCES

Anand, M., & Sinha, A.K. (2012). Temperature-Dependent Reaction Pathways for the Anomalous Hydrocracking of Triglycerides in the Presence of Sulfided Co–Mo–catalyst. Bioresour Technol, 126, 148–155. https ://doi.org/10.1016/j.biort ech.2012.08.105

Anjani, R. K., Gollakota, M., & Subramanyam, D. (2015). CFD Simulations on the Effect of Catalysts on the Hydrodeoxygenation of Bio-Oil, Royal Society of Chemistry, 5, 41855. https://doi.org/10.1039/C5RA02626A

CPL Press (n.d.). Newbury, UK, Vol. 1. https://www.osti.gov/etdeweb/biblio/20133955

Edward, F. (1983). Chemistry of Catalytic Hydrodeoxygenation, Catalysis Review, 25, UK, 421 - 458. https://doi.org/10.1080/01614948308078052

Elkasabi, Y., & Mullen, C. A. (2014). Hydrodeoxygenation of Fast Pyrolysis Bio – Oils from Various Feedstocks Using Carbon – Supported Catalysts, Fuel Processing Technology, 123, 11-18. https://doi.org/10.1016/j.fuproc.2014.01.039

Guardo, A., & Casanovas, M. (2007). CFD Modeling on External Mass Transfer and Intra- Particle Diffusional Effects on the Supercritical Hydrogenation of Sunflower Oil, Chemical Engineering Science 62, 5054–5061. https://doi.org/10.1016/j.ces.2007.01.080

Gutiérrez, A., & Kaila, R. K. (2009). Hydrodeoxygenation of Guaiacol on Noble Metal Catalysts, Catalysis Today, 147(3-4), 239–246. https://doi.org/10.1016/j.cattod.2008.10.037

Mahfud, F. H. (2007). Hydrotreatment of Fast Pyrolysis Oil Using Heterogeneous Noble Metal Catalysts, PhD Thesis, University of Gronigen : A Handbook, CPL Press, Newbury, UK, vol. 1. https://doi.org/10.1021/ie9006003

Mederos, N. F., Elizalde, M, I., Trejo, Z. F. (2020). Dynamic Modeling and Simulation of Three-Phase Reactors for Hydrocracking of Vegetable Oils, Reaction Kinetics, Mechanisms and Catalysis 131, 613 – 644. https://doi.org/10.1007/s11144-020-01896-4

Mendoza, C. C., & Vélez, J. F. (2015). CFD Analysis of the Heat Transfer Coefficient During Hydrotreatment of Palm Oil, 08 -12-2015, V Symposium Internacional de Biofábricas, virtual. DOI: 10.1039/c5ra14985a

Mortensen, P. M., Grunwaldt, J. D., Jensen, P. A., Knudsen, K. G., & Jensen, A. D.=. (2011). A review of Catalytic Upgrading of Bio – Oil to Engines Fuels, Applied Catalysis A: general, 407, 1-19. https://doi.org/10.1016/j.apcata.2011.08.046

Muharam, Y., & Putri, A. D. (2019). Phenomenological Model for the Prediction of the Performance of a Slurry Bubble Column Reactor for Green Diesel Production, Journal of physics: Conference series, 1349, 012057. DOI 10.1088/1742-6596/1349/1/012057

Muharam, Y., Nugraha, O. A. (2017). Modelling of a Hydrotreating Reactor to Produce Renewable Diesel from Non-Edible Vegetable Oils, Chemical Engineering Transactions, 56, 1561 – 1566. https://doi.org/10.3303/CET1756261

Oasmaa, A., Meier, D., & Bridgwater, A. (2002). Fast Pyrolysis of Biomass: A Handbook, ANSYS, Inc., (2016), ANSYS Fluent User's Guide. Canonsburg, PA, USA.

Oyama, S. T. (1996). The Chemistry of Transition Metal Carbides and Nitrides. Blackie Academic and Professional, Springer, Virginia, USA. https://DOI: 10.1007/978-94-009-1565- 7_1

Subramanyam, M. D. (2015), CFD Simulations of Catalytic Hydrodeoxygenation of Bio – Oil Using Pt/Al2O3 in a Fixed Bed Reactor, RSC Advances, 110, 90354 – 90366.

Wildschut, J., & Mahfud, F. H. (2009). Hydrotreatment of Fast Pyrolysis Oil Using Heterogeneous Noble - Metal Catalysts, Ind. Eng. Chem. Res., 48(23), 1324–1334. https://doi.org/10.1021/ie9006003

Wildschut, J., & Melian – Cabrera, I. (2010). Catalyst Studies on the Hydrotreatment of Fast Pyrolysis oil, Applied Catalysis B: Environmental, 99(1 -2), 298 – 306. https://doi.org/10.1016/j.apcatb.2010.06.036